Wiley
Journal of Mathematics
Volume 2024, Article ID 4598831, 14 pages
https://doi.org/10.1155/2024/4598831

WILEY

Research Article

The Exact Solutions of a Diffusive SIR Model via Symmetry Groups

R. Naz,[1] **A. G. Johnpillai**,[2] **and F. M. Mahomed**[3]

[1]*Department of Mathematics and Statistical Sciences, Lahore School of Economics, Lahore 53200, Pakistan*
[2]*Department of Mathematics, Eastern University Sri Lanka, Chenkaladi 30350, Sri Lanka*
[3]*DSI-NRF Centre of Excellence in Mathematical and Statistical Sciences, School of Computer Science and Applied Mathematics, University of the Witwatersrand, Johannesburg, Wits 2050, South Africa*

Correspondence should be addressed to F. M. Mahomed; fazal.mahomed@wits.ac.za

Received 26 November 2023; Revised 7 April 2024; Accepted 22 April 2024

Academic Editor: Antonio Di Crescenzo

The focus of this paper is to investigate the exact solutions of a diffusive susceptible-infectious-recovered (SIR) epidemic model, characterized by a nonlinear incidence. A four-dimensional Lie point symmetry algebra is obtained for this model. We utilize the Lie symmetries to deduce the optimal system of one-dimensional subalgebras. The reductions and group-invariant solutions are obtained with the aid of these subalgebras. We also derive new group-invariant solutions and reductions for the underlying model via subalgebras that are related to the optimal system by adjoint maps. We developed the diffusive susceptible-infectious-quarantined (SIQ) model with quarantine-adjusted incidence function to understand the transmission dynamics of COVID-19.

1. Introduction

Models of epidemiology have been of great interest, and different mathematical approaches have been utilized for their analysis and solutions. The SIR model, as presented in Kermack and McKendrick [1], and its adaptations are often used in multiple studies dealing with epidemiological models. A natural extension of the classical Kermack and McKendrick model involves understanding the spatial dynamics of disease spread. We present some works that are of relevance here. The geographic and temporal expansion of plagues investigated by Noble [2] provides the foundation for subsequent research in this area. Reaction-diffusion equations were employed to explore the diffusion of rabies among red foxes across Europe [3–6]. We refer the reader to comprehensive surveys [7, 8] and reference therein for the pioneering works to understand the spatial dynamics of disease spread.

Fu [9] established the traveling waves for a diffusive SIR model with delay. The traveling wave solutions of different variants of a delayed SIR model with diffusion were studied by Yang et al. [10], Zhou et al. [11], and Zhen et al. [12]. Investigating a diffusive SIR epidemic model in a spatially heterogeneous environment, the study [13] delves into the dynamics, global stability, and impact of heterogeneity on disease persistence, demonstrating that even with a basic reproduction number less than 1, high initial infective numbers could sustain the disease. Exploring time-periodic traveling wave solutions in a periodic SIR epidemic model with diffusion and nonlinear incidence, Wang et al. [14] demonstrate the existence of these waves by examining fixed points of a nonlinear operator on a set of periodic functions. Moreover, utilizing comparison arguments and properties of spreading speeds, the study establishes the nonexistence of certain periodic traveling waves. The work of Zhou et al. [15] demonstrates the novel achievement of obtaining a nontrivial, positive, and bounded critical traveling wave solution for a diffusive disease model with an infinite equilibrium reaction system, resolving an open question as discussed in Wang et al. [14]. The critical traveling wave is revealed as a hybrid of both front and pulse types. Zhao et al. [16] explored the existence and nonexistence of traveling waves in a two-group diffusive SIR epidemic model. It was shown that the system permits nontrivial traveling wave solutions when the basic reproduction number is greater than 1 and no nontrivial traveling waves are found for the case when the basic reproduction number is less than or equal to 1. Cao et al. [17] studied a diffusive SIR epidemic model with a saturated incidence rate. Thabet and Kendre [18] studied the diffusive SIR model and a diffusive susceptible-exposed-infected-recovered-deceased (SEIRD) model based on conformable space-time PDEs to understand the transmission dynamics of COVID-19.

We investigate the epidemic model previously analyzed by Wang et al. [14] and Zhao et al. [16] employing the perspective of Lie point symmetries. The Lie symmetry approach to a differential equation is systematic and results in reductions and solutions in an algorithmic manner (see e.g., the books [19–24]). There are efficient computer packages which have been developed for the computation of Lie symmetries (see e.g., [25–31]). There has been a paucity of investigations on the exact solution to the epidemic models. The symmetry approach [32–35] has been useful in the application to the spatio-temporal epidemic models represented by partial differential equations (PDEs) in order to obtain Lie symmetries as well as exact solutions to these models. We utilize the Lie symmetry method for the SIR model. For equal diffusion rates, the Lie symmetry algebra is four-dimensional. This leads us to derive symmetry reductions and group-invariant solutions by utilizing an optimal system of one-dimensional subalgebras. Further relevant group-invariant solutions and reductions of the model are derived by subalgebras that are adjoint maps from the optimal system. The newly obtained exact solutions significantly differ from the traveling wave solutions previously reported by Wang et al. [14] and Zhou et al. [15]. To illustrate the implications of our findings, we developed a diffusive SIQ model with a quarantine-adjusted incidence function.

The outline of this paper is as follows. In Section 2, the Lie point symmetry algebras for the epidemic model with the same or equal diffusion rates are determined to be four-dimensional. The optimal system of one-dimensional subalgebras is then deduced. We present the symmetry reductions and group-invariant solutions of the model understudy with equal diffusion rates obtained directly by the optimal system of one-dimensional subalgebras. Section 3 deals with group-invariant solutions obtained by means of other subalgebras related to the optimal system by adjoint maps. The exact solutions for the diffusive SIQ model are provided in Section 4. Section 5 contains the final concluding remarks.

2. A Diffusive Susceptible-Infectious-Recovered (SIR) Epidemic Model

Let t represents time and x is a spatial coordinate representing the position in a one-dimensional space. The variables $S(t,x)$, $I(t,x)$, and $R(t,x)$ describe the densities of the susceptible, infected, and recovered populations, respectively, at different points in time t and space x. The focal point of the study [14] was the following diffusive SIR epidemic model with nonlinear incidence:

$$S_t = d_1 S_{xx} - \frac{\beta SI}{S+I}, \tag{1}$$

$$I_t = d_2 I_{xx} + \frac{\beta SI}{S+I} - \gamma I, \tag{2}$$

$$R_t = d_3 R_{xx} + \gamma I, \tag{3}$$

where the positive constants β, γ, and d_i denote the infection rate, the recovery rate, and the diffusion rates, respectively. Here, we consider the equal diffusion rate case $d_1 = d_2 = d_3 = \delta$. Henceforth, we focus on the equal or same diffusion rate δ. The total population is $N = S + I + R$. Systems (1)–(3) for the equal diffusion case $d_1 = d_2 = d_3 = \delta$ take the following form:

$$S_t = \delta S_{xx} - \frac{\beta SI}{S+I}, \tag{4}$$

$$I_t = \delta I_{xx} + \frac{\beta SI}{S+I} - \gamma I, \tag{5}$$

$$N_t = \delta N_{xx}, \tag{6}$$

and $R = N - S - I$. There are different approaches in finding solutions of systems (4)–(6), qualitative, approximate, and exact. We utilize the Lie symmetry method which is well known in the vast literature with many recent applications using this effective method. Since N does not appear in the first two equations in systems (4) to (6), we can focus on the subsystem of equations (4) and (5) in our analysis. The solution for N results in a diffusion equation (6) which have well-known solutions and $R = N - S - I$.

2.1. Optimal System of One-Dimensional Subalgebras. We establish the Lie symmetries of the subsystem of equations (4) and (5) by utilizing the Maple-based packages [27, 28] which yield the following Lie symmetries:

$$\begin{aligned} X_1 &= \partial_t, \\ X_2 &= \partial_x, \\ X_3 &= S\partial_S + I\partial_I, \\ X_4 &= 2\delta t\partial_x - xS\partial_S - xI\partial_I. \end{aligned} \tag{7}$$

It is worth mentioning here that the Lie algebra of invariance (7) for equations (4) and (5) is the classical Galilei algebra, a common feature in equations found in real-world applications, but here, it emerges in the context of the epidemic model. All possible reaction-diffusion systems invariant under this algebra were described in [36]. Equations (4) and (5) represent a specific case of the general form of Galilei-invariant systems of PDEs presented in [36]. The commutation relations of the four-dimensional Lie algebra of the subsystem of PDEs (4) and (5) are presented in Table 1.

To obtain the reduced system of ODEs using symmetries and hence to construct classes of group-invariant solutions for the system of PDEs (4) and (5) in a systematic manner,

Table 1: Commutation relations for 4-dimensional Lie algebra of subsystems (4) and (5).

[,]	X_1	X_2	X_3	X_4
X_1	0	0	0	$2\delta X_2$
X_2	0	0	0	$-X_3$
X_3	0	0	0	0
X_4	$-2\delta X_2$	X_3	0	0

one resorts to the optimal system of one-dimensional subalgebras for the underlying system. The method employed to construct an optimal system of one-dimensional subalgebras is well known and detailed in [19, 21], among other related works.

To compute the adjoint representation, we utilize the commutation relations in Table 1 and the following well-known Lie series (see e.g., [19, 21]):

$$\mathrm{Ad}(\exp(\epsilon X))Y = Y - \epsilon[X,Y] + \frac{1}{2!}\epsilon^2[X,[X,Y]] - \frac{1}{3!}\epsilon^3[X,[X,[X,Y]]] + \ldots. \tag{8}$$

For example,

$$\begin{aligned}\mathrm{Ad}(\exp(\epsilon X_1))X_4 &= X_4 - \epsilon[X_1,X_4] + \frac{1}{2!}\epsilon^2[X_1,[X_1,X_4]] - \ldots\\ &= X_4 - 2\delta\epsilon X_2.\end{aligned} \tag{9}$$

Likewise, determining the remaining entries of the adjoint table is straightforward. Table 2 presents the complete adjoint representation. The entry (i,j) gives the action of the adjoint operator $\mathrm{Ad}(\exp(\epsilon X_i))X_j$. Considering a nonzero vector represented as

$$X = a_1X_1 + a_2X_2 + a_3X_3 + a_4X_4, \tag{10}$$

we aim to simplify X by annulling and setting the coefficients a_i to unity wherever feasible, through adjoint mappings. The calculations are straightforward, leading to the derivation of an optimal system of one-dimensional subalgebras spanned by

$$X_2, X_3, X_4 + \lambda X_1, X_1 + \mu X_3, \tag{11}$$

where λ and μ are constants. It is important to mention here that our optimal system is equivalent to that given in [37]. We mention the results without calculations as these are utilized.

Next, we present the reductions and solutions to the above optimal system of subalgebras and those that map to these by adjoint action in Section 3.

2.2. Exact Solution Using X_2. The invariance surface conditions, [19, 23], yield

$$\begin{aligned}S_x &= 0,\\ I_x &= 0.\end{aligned} \tag{12}$$

Equation (12) provides the group-invariant solutions $S = f(y)$ and $I = g(y)$, where $y = t$, which reduces the system of PDEs (4) and (5) to the following system of nonlinear first-order ODEs

$$\begin{aligned}f' + \frac{\beta f g}{f+g} &= 0,\\ g' - \frac{\beta f g}{f+g} + \gamma g &= 0,\end{aligned} \tag{13}$$

where prime denotes differentiation with respect to y.

From the first equation of (13), we obtain

$$g = \frac{-ff'}{f' + \beta f}. \tag{14}$$

We substitute (14) and its derivative into the second equation of (13), which results in the nonlinear second-order ODE

$$-\beta f^2 f'' = (\gamma - 2\beta) f f'^2 + \beta(\gamma - \beta) f^2 f'. \tag{15}$$

2.2.1. Case $(\gamma \neq 2\beta)$ and $(\gamma \neq \beta)$. The solution of this second order ODE is

$$f(t) = \left(\frac{A_2(\gamma - \beta) - A_1 e^{(\beta-\gamma)t}}{\beta}\right)^{(\beta/(\gamma-\beta))} \tag{16}$$

and

$$g(t) = \frac{A_1}{A_2(\beta - \gamma)} e^{(\beta-\gamma)t}\left(\frac{A_2(\gamma - \beta) - A_1 e^{(\beta-\gamma)t}}{\beta}\right)^{(\beta/(\gamma-\beta))}. \tag{17}$$

Thus, $S(t,x) = f(t)$ and $I(t,x) = g(t)$ which is the same as [39] for the model with no diffusion. The last equation is

Table 2: Adjoint table of Lie algebra of the subsystem of equations (4) and (5).

Ad	X_1	X_2	X_3	X_4
X_1	X_1	X_2	X_3	$X_4 - \epsilon 2\delta X_2$
X_2	X_1	X_2	X_3	$X_4 + \epsilon X_3$
X_3	X_1	X_2	X_3	X_4
X_4	$X_1 + \epsilon 2\delta X_2 - \epsilon^2 \delta X_3$	$X_2 - \epsilon X_3$	X_3	X_4

$$N_t = \delta N_{xx}, \tag{18}$$

and $R = N - S - I$.

2.2.2. (*Case* $\gamma = 2\beta$). Case 1 ($\gamma = 2\beta$). In this case, equation (15) reduces to $f' + (\gamma/2)f = c_1$, where c_1 is an arbitrary constant. The general solution of this equation is given by

$$f(y) = \frac{2c_1}{\gamma} + c_2 e^{(-\gamma/2)y}. \tag{19}$$

Substitution of the solution (19) into (14) yields the following group-invariant solutions:

$$S = \frac{2c_1}{\gamma} + c_2 e^{(-\gamma/2)t}, I = c_2 e^{(-\gamma/2)t} + \frac{\gamma c_2^2}{2c_1} e^{(-\gamma/2)t}. \tag{20}$$

2.2.3. (*Case* $\gamma = \beta$). Case 2 ($\gamma = \beta$). Here, equation (15) reduces to $ff'' - f'^2 = 0$. The general solution of this equation is given by

$$f(y) = c_2 e^{c_1 y}, \tag{21}$$

where c_1 and c_2 are arbitrary constants. By substitution of the solution (21) into (14), we deduce the following group-invariant solutions

$$S = c_1 c_2 e^{c_1 t}, I = \frac{-c_1 c_2^2 e^{c_1 t}}{c_2 (c_1 + \gamma)}. \tag{22}$$

2.3. Reduction Using X_3. The generator X_3 does not provide any nontrivial group-invariant solutions and reductions to the system of PDEs (4) and (5) as is evident.

2.4. Reduction Using $X_1 + \mu X_3$. The invariance surface conditions, [19, 23], yield

$$\begin{aligned} S_t &= \mu S, \\ I_t &= \mu I. \end{aligned} \tag{23}$$

Equation (23) provides the group-invariant solutions $S = f(x)e^{\mu t}$ and $I = g(x)e^{\mu t}$ which yield the reduction of the system of PDEs (4) and (5) to a coupled nonlinear system of second-order ODEs

$$\begin{aligned} \delta f'' - \beta \frac{fg}{f+g} - \mu f &= 0, \\ \delta g'' + \beta \frac{fg}{f+g} - (\mu + \gamma) g &= 0, \end{aligned} \tag{24}$$

where prime refers to differentiation with respect to x. Numerical solutions for the system of second-order ODEs (24) can be obtained using appropriate numerical techniques. Our main goal is to derive exact solutions, and we avoid exploring approximate or numerical solutions in this study.

2.5. Reduction Using $X_4 + \lambda X_1$. The $X_4 + \lambda X_1$-invariant solutions, $S = e^{(-tx/\lambda) + (2at^3/3\lambda^2)} f(y)$ and $I = e^{(-tx/\lambda) + (2at^3/3\lambda^2)} g(y)$, where $y = x - (at^2/\lambda)$, reduce the system of PDEs (4) and (5) to the following system of nonlinear second-order ODEs:

$$\begin{aligned} \delta f'' + \frac{y}{\lambda} f - \frac{\beta f g}{f+g} &= 0, \\ \delta g'' + \left(\frac{y}{\lambda} - \gamma\right) g + \frac{\beta f g}{f+g} &= 0, \end{aligned} \tag{25}$$

where again prime denotes differentiation with respect to y. One can use numerical techniques to find solutions for the system of second-order ordinary differential equations (25).

3. Exact Solution for Lie Subalgebras Related to the Optimal System

In this section, we consider other Lie subalgebras contained in the optimal system through adjoint maps. Finding exact solutions for the second-order nonlinear ODEs (24) and (25) is a highly nontrivial problem. Thus, we look at such reductions via Lie symmetries that result in the first-order ODEs. We establish many relevant exact solutions.

3.1. Exact Solutions Using Lie Symmetries X_2 *and* X_3. Here, we consider the group-invariant solution invariant under $X_2 + \eta_1 X_3$. These solutions are related to those invariants under X_2 via the adjoint map as $\mathrm{Ad}(\exp(-\eta_1 X_4))X_2 = X_2 + \eta_1 X_3$. This combination of Lie symmetries $X_2 + \eta_1 X_3$ then yields the following group invariant solution:

$$\begin{aligned} S(t,x) &= F_1(t) e^{\eta_1 x}, \\ I(t,x) &= F_2(t) e^{\eta_1 x}, \end{aligned} \tag{26}$$

where $F_1(t)$ and $F_2(t)$ satisfy the following system of ordinary differential equations:

$$\begin{aligned} (F_1 + F_2)F_1' - \delta\eta_1^2 F_1^2 - \left(\delta\eta_1^2 - \beta\right) F_1 F_2 &= 0, \\ (F_1 + F_2)F_2' - \left(\delta\eta_1^2 - \gamma\right) F_2^2 - \left(\delta\eta_1^2 + \beta - \gamma\right) F_1 F_2 &= 0. \end{aligned} \tag{27}$$

The exact solution of system of ODEs (27) is given by

$$F_1(t) = e^{(\delta\eta_1^2-\beta)t}\left(\frac{A_2 - A_1 e^{-(\beta-\gamma)t}}{\beta}\right)^{-(\beta/(\beta-\gamma))},$$
$$F_2(t) = -e^{(\delta\eta_1^2-\gamma)t}\left(\frac{A_2 - A_1 e^{-(\beta-\gamma)t}}{\beta}\right)^{-(\beta/(\beta-\gamma))}\frac{A_2}{A_1}, \tag{28}$$

where A_1 and A_2 are arbitrary constants of integration. Upon substituting $F_1(t)$ and $F_2(t)$ from (28) into (26), we arrive at the final form of the group-invariant solution for $S(t,x)$ and $I(t,x)$

$$S(t,x) = e^{(\delta\eta_1^2-\beta)t+\eta_1 x}\left(\frac{A_2 - A_1 e^{-(\beta-\gamma)t}}{\beta}\right)^{-(\beta/(\beta-\gamma))},$$
$$I(t,x) = -e^{(\delta\eta_1^2-\gamma)t+\eta_1 x}\left(\frac{A_2 - A_1 e^{-(\beta-\gamma)t}}{\beta}\right)^{-(\beta/(\beta-\gamma))}\frac{A_2}{A_1}. \tag{29}$$

The solutions of the diffusion equation for the total population

$$N_t = \delta N_{xx}, \tag{30}$$

is well known and finally $R = N - S - I$. This completes the exact solution for all the variables of the SIR model. It is important to mention here that the group-invariant solution (29) holds for $\eta_1 = 0$ case as well. This is equivalent to solving the system of PDEs via X_2 discussed in Subsection 2.2 wherein we considered special cases as well.

3.2. Exact Solutions Using Lie Symmetries X_2 and X_4. The exact solution invariant under $X_2 + \eta_2 X_4$ is recovered by the adjoint action on X_4 by $\mathrm{Ad}(\exp X_1)$. The combination $X_2 + \eta_2 X_4$ yields the following group-invariant solution:

$$S(t,x) = F_3(t)e^{-\left(\eta_2 x^2/4\eta_2\delta t+2\right)},$$
$$I(t,x) = F_4(t)e^{-\left(\eta_2 x^2/4\eta_2\delta t+2\right)}, \tag{31}$$

where $F_3(t)$ and $F_4(t)$ satisfy

$$(F_3+F_4)\left(\eta_2\delta t+\frac{1}{2}\right)F_3' + \frac{1}{2}\delta\eta_2 F_3^2 + \left(\delta\beta\eta_2 t + \frac{1}{2}\eta_2\delta + \frac{1}{2}\beta\right)F_3F_4 = 0,$$
$$(F_3+F_4)\left(\eta_2\delta t+\frac{1}{2}\right)F_4' + \left(\gamma\delta\eta_2 t + \frac{1}{2}\delta\eta_2 + \frac{1}{2}\gamma\right)F_4^2 + \left(\frac{1}{2}\delta\eta_2 - \beta\delta\eta_2 t + \gamma\delta\eta_2 t + \frac{1}{2}\gamma - \frac{1}{2}\beta\right)F_3F_4 = 0. \tag{32}$$

The exact solution of system of ODEs (32) is given by

$$F_3(t) = \frac{\left(e^{(\beta-\gamma)t}A_3 - A_4\right)^{-(\beta/(\beta-\gamma))}\beta^{(\beta/(\beta-\gamma))}}{\sqrt{2\eta_2\delta t+1}},$$
$$F_4(t) = -\frac{\left(e^{(\beta-\gamma)t}A_3 - A_4\right)^{-(\beta/(\beta-\gamma))}e^{(\beta-\gamma)t}\beta^{(\beta/(\beta-\gamma))}A_3}{\sqrt{2\eta_2\delta t+1}A_4}, \tag{33}$$

where A_3 and A_4 are arbitrary constants of integration. Upon substituting $F_3(t)$ and $F_4(t)$ from (31) into (33), we arrive at the final form of the group-invariant solution for $S(t,x)$ and $I(t,x)$

$$S(t,x) = \frac{\left(e^{(\beta-\gamma)t}A_3 - A_4\right)^{-(\beta/(\beta-\gamma))}\beta^{(\beta/(\beta-\gamma))}e^{-\left(\eta_2 x^2/4\eta_2\delta t+2\right)}}{\sqrt{2\eta_2\delta t+1}},$$
$$I(t,x) = -\frac{\left(e^{(\beta-\gamma)t}A_3 - A_4\right)^{-(\beta/(\beta-\gamma))}e^{(\beta-\gamma)t}A_3\beta^{(\beta/(\beta-\gamma))}e^{-\left(\eta_2 x^2/4\eta_2\delta t+2\right)}}{\sqrt{2\eta_2\delta t+1}A_4}. \tag{34}$$

The solutions of the diffusion equation for the total population $N_t = \delta N_{xx}$ is again known and $R = N - S - I$. This completes the exact solution for all the variables of the SIR model.

3.3. Exact Solutions Using Lie Symmetries X_3 and X_4. The following group invariant solution arises from the combination of Lie symmetries $X_4 + \eta_3 X_3$ (the adjoint map $\mathrm{Ad}(\exp \eta_3 X_2)X_4 = X_4 + \eta_3 X_3$):

$$S(t,x) = F_5(t)e^{(x(2\eta_3 - x)/4t\delta)},$$
$$I(t,x) = F_6(t)e^{(x(2\eta_3 - x)/4t\delta)}, \tag{35}$$

where $F_5(t)$ and $F_6(t)$ satisfy the system of ODEs

$$t^2\delta(F_5+F_6)F_5' + \left(\frac{1}{2}t\delta - \frac{1}{4}\eta_3^2\right)F_5^2 + \left(t^2\beta\delta + \frac{1}{2}t\delta - \frac{1}{4}\eta_3^2\right)F_5F_6 = 0,$$
$$t^2\delta(F_5+F_6)F_6' + \left(t^2\delta\gamma + \frac{1}{2}t\delta - \frac{1}{4}\eta_3^2\right)F_6^2 + \left[\left(\frac{1}{2} - \beta t + \gamma t\right)\delta t - \frac{1}{4}\eta_3^2\right]F_5F_6 = 0. \tag{36}$$

The exact solution of system of ODEs (36) is given by

$$F_5(t) = \frac{\left(e^{(\beta-\gamma)t}A_5 - A_6\right)^{-(\beta/(\beta-\gamma))}\beta^{(\beta/(\beta-\gamma))}e^{-\left(\eta_3^2/4t\delta\right)}}{\sqrt{t}},$$
$$F_6(t) = -\frac{e^{\left(4\beta\delta t^2 - 4\gamma\delta t^2 - \eta_3^2/4t\delta\right)}A_5\beta^{(\beta/(\beta-\gamma))}\left(e^{(\beta-\gamma)t}A_5 - A_6\right)^{-(\beta/(\beta-\gamma))}}{A_6\sqrt{t}}, \tag{37}$$

where A_5 and A_6 are arbitrary constants of integration. Upon substituting $F_5(t)$ and $F_6(t)$ from (35) into (37), we arrive at the final form of the group-invariant solution for $S(t,x)$ and $I(t,x)$

$$S(t,x) = \frac{\left(e^{(\beta-\gamma)t}A_5 - A_6\right)^{-(\beta/(\beta-\gamma))}\beta^{(\beta/(\beta-\gamma))}e^{-\left(\eta_3^2 - 2\eta_3 x + x^2/4t\delta\right)}}{\sqrt{t}},$$
$$I(t,x) = -\frac{e^{\left(4\beta\delta t^2 - 4\gamma\delta t^2 - \eta_3^2 + 2\eta_3 x - x^2/4t\delta\right)}A_5\beta^{(\beta/(\beta-\gamma))}\left(e^{(\beta-\gamma)t}A_5 - A_6\right)^{-(\beta/(\beta-\gamma))}}{A_6\sqrt{t}}. \tag{38}$$

Again, the solutions of the diffusion equation for the total population are known and $R = N - S - I$. This completes the exact solution for all the variables of the SIR model. It is important to mention here that the group-invariant solution (38) holds for $\eta_3 = 0$ case as well. This is equivalent to solving the system of PDEs via X_4.

4. Analyzing COVID-19 Transmission Dynamics through the Diffusive SIQ Model with Quarantine-Adjusted Incidence

In this section, we relate the derived results to a real-world scenario. The appropriate initial and boundary conditions are considered. If we replace the compartment representing recovered or removed individuals with a quarantine compartment denoted as $Q(t,x)$, the system described by equations (1)–(3) can be interpreted as a diffusive SIQ model with a quarantine-adjusted incidence function. Specifically, we assume no movement of individuals in the quarantine class between compartments, leading to $d_3 = 0$, and we consider the equal diffusion rate case $d_1 = d_2 = \delta$. The resulting model is as follows:

$$S_t = \delta S_{xx} - \frac{\beta SI}{S+I}, \tag{39}$$

$$I_t = \delta I_{xx} + \frac{\beta SI}{S+I} - \gamma I, \tag{40}$$

$$Q_t = \gamma I, \tag{41}$$

where the parameters are defined as $\beta > 0$ is the contact rate of susceptible individuals with infected individuals, $\gamma > 0$ is the isolation rate of infected individuals, and δ is the diffusion rate. The actively mixing population-representing individuals with whom a susceptible person can come into contact are defined as $N - Q = S + I$ (see e.g., Hethcote et al. [38] and Naz and Al-Raeei [39]). The quarantine-adjusted incidence function, denoted as $((\beta SI)/S + I)$, is derived by substituting the denominator N in the standard incidence formula $((\beta SI)/N)$ with the actively mixed population $N-Q=S+I$. Consequently, the force of infection is expressed as $(\beta I)/(S+I)$. The reproductive number for this model is $\rho_0=\beta/\gamma$. Upon closer examination, it becomes evident that the diffusive SIQ model (39)–(41) is identical to (4)–(6) for $d_3=0$ case. We will utilize this model to study the transmission dynamics of COVID 19.

A similar procedure, as outlined in Sections 2 and 3, could be carried out to obtain reductions and exact solutions for the variables $S(t,x)$ and $I(t,x)$ within the subsystem of equations (39) and (40). Subsystems (39) and (40) are identical to subsystems (4) and (5); therefore, the reductions and exact solutions developed in Sections 2 and 3 for the variables S and I remain applicable to the subsystem of equations (39) and (40). For the diffusive SIQ model, the variable Q from equation (41) is

$$Q(t,x)=\gamma\int_0^t I(\tau,x)\mathrm{d}\tau+F(x), \tag{42}$$

where $F(x)$ is an arbitrary function of x and τ is the dummy variable. We consider the appropriate initial and boundary conditions to further analyze this model to study the transmission dynamics of COVID-19.

4.1. Initial and Boundary Conditions. The initial conditions are specified as follows:

$$\begin{aligned} S(0,x)&=S_0\Lambda(x), \quad 0\le x\le L,\\ I(0,x)&=I_0\Lambda(x), \quad 0\le x\le L,\\ Q(0,x)&=Q_0\Lambda(x), \quad 0\le x\le L, \end{aligned} \tag{43}$$

where S_0, I_0, and Q_0 are constants that scale the initial distributions of susceptible, infected, and quarantined individuals, respectively. The function $\Lambda(x)$ describes the initial spatial distributions of susceptible, infected, and quarantine individuals. We investigate a scenario with time-dependent nonhomogeneous Dirichlet boundary conditions at $x=0$ and $x=L$:

$$\begin{aligned} S(t,0)&=\Omega_1(t), \quad 0\le t\le T,\\ I(t,0)&=\Omega_2(t), \quad 0\le t\le T,\\ Q(t,0)&=\Omega_3(t), \quad 0\le t\le T,\\ S(t,L)&=\Omega_4(t), \quad 0\le t\le T,\\ I(t,L)&=\Omega_5(t), \quad 0\le t\le T,\\ Q(t,L)&=\Omega_6(t), \quad 0\le t\le T. \end{aligned} \tag{44}$$

The following compatibility conditions must hold:

$$\begin{aligned} &S_0\Lambda(0)=\Omega_1(0), I_0\Lambda(0)=\Omega_2(0), Q_0\Lambda(0)=\Omega_3(0),\\ &S_0\Lambda(L)=\Omega_4(0), I_0\Lambda(L)=\Omega_5(0), Q_0\Lambda(L)=\Omega_6(0). \end{aligned} \tag{45}$$

It is worth mentioning that the exact solution for variables $S(t,x)$ and $I(t,x)$ provided in equations (29), (34), and (38) involves both variables t and x. Is it possible to find an exact solution subject to the initial conditions (43) and boundary conditions (44)? We utilize the combination of Lie symmetries $X_2-\eta X_3$ outlined in Subsection 3.1 with $\eta_1=-\eta$ and establish the exact solution for variables $S(t,x)$ and $I(t,x)$ subject to initial and boundary conditions. Applying the initial conditions (43) to the group-invariant solution (26) yields

$$F_1(0)=S_0, F_2(0)=I_0, \tag{46}$$

and

$$\Lambda(x)=e^{-\eta x}. \tag{47}$$

The exact solution of the system of ODEs (27) subject to initial conditions (46) is given by

$$\begin{aligned} F_1(t)&=S_0e^{(\delta\eta^2-\beta)t}\left(\frac{I_0+S_0e^{-(\beta-\gamma)t}}{S_0+I_0}\right)^{-(\beta/(\beta-\gamma))},\\ F_2(t)&=I_0e^{(\delta\eta^2-\gamma)t}\left(\frac{I_0+S_0e^{-(\beta-\gamma)t}}{S_0+I_0}\right)^{-(\beta/(\beta-\gamma))}. \end{aligned} \tag{48}$$

By substituting $F_1(t)$ and $F_2(t)$ from (48) into (26), we obtain the final form of the group-invariant for the variables $S(t,x)$ and $I(t,x)$ as follows:

$$\begin{aligned} S(t,x)&=S_0e^{(\delta\eta^2-\beta)t-\eta x}\left(\frac{I_0+S_0e^{-(\beta-\gamma)t}}{S_0+I_0}\right)^{-(\beta/(\beta-\gamma))},\\ I(t,x)&=I_0e^{(\delta\eta^2-\gamma)t-\eta x}\left(\frac{I_0+S_0e^{-(\beta-\gamma)t}}{S_0+I_0}\right)^{-(\beta/(\beta-\gamma))}. \end{aligned} \tag{49}$$

The variable $Q(t,x)$, as given in equation (42), takes the following form:

$$Q(t,x)=\gamma\int_0^t\left(I_0e^{(\delta\eta^2-\gamma)\tau-\eta x}\left(\frac{I_0+S_0e^{-(\beta-\gamma)\tau}}{S_0+I_0}\right)^{-(\beta/(\beta-\gamma))}\right)\mathrm{d}\tau+Q_0e^{-\eta x}, \tag{50}$$

with $F(x) = Q_0 e^{-\eta x}$ ensures that $Q(t, x)$ satisfies the specified initial condition. Next, we apply the boundary conditions (44) and arrive at the following expressions for $\Omega_i(t)$, $i = 1, \ldots, 6$

$$
\begin{aligned}
\Omega_1(t) &= S_0 e^{(\delta\eta^2-\beta)t}\left(\frac{I_0 + S_0 e^{-(\beta-\gamma)t}}{S_0 + I_0}\right)^{-(\beta/(\beta-\gamma))}, \quad 0 \le t \le T,\\
\Omega_2(t) &= I_0 e^{(\delta\eta^2-\gamma)t}\left(\frac{I_0 + S_0 e^{-(\beta-\gamma)t}}{S_0 + I_0}\right)^{-(\beta/(\beta-\gamma))}, \quad 0 \le t \le T,\\
\Omega_3(t) &= \gamma \int_0^t \left(I_0 e^{(\delta\eta^2-\gamma)\tau}\left(\frac{I_0 + S_0 e^{-(\beta-\gamma)\tau}}{S_0 + I_0}\right)^{-(\beta/(\beta-\gamma))}\right) d\tau + Q_0, \quad 0 \le t \le T,\\
\Omega_4(t) &= S_0 e^{(\delta\eta^2-\beta)t-\eta L}\left(\frac{I_0 + S_0 e^{-(\beta-\gamma)t}}{S_0 + I_0}\right)^{-(\beta/(\beta-\gamma))}, \quad 0 \le t \le T,\\
\Omega_5(t) &= I_0 e^{(\delta\eta^2-\gamma)t-\eta L}\left(\frac{I_0 + S_0 e^{-(\beta-\gamma)t}}{S_0 + I_0}\right)^{-(\beta/(\beta-\gamma))}, \quad 0 \le t \le T,\\
\Omega_6(t) &= \gamma \int_0^t \left(I_0 e^{(\delta\eta^2-\gamma)\tau-\eta L}\left(\frac{I_0 + S_0 e^{-(\beta-\gamma)\tau}}{S_0 + I_0}\right)^{-(\beta/(\beta-\gamma))}\right) d\tau + Q_0 e^{-\eta L}, \quad 0 \le t \le T.
\end{aligned}
\tag{51}
$$

The final form of the exact solution for the diffusive SIQ model (39)–(41), which satisfies the initial conditions (43), boundary conditions (44), and compatibility conditions (45), is given by

$$
\begin{aligned}
S(t,x) &= S_0 e^{(\delta\eta^2-\beta)t-\eta x}\left(\frac{I_0 + S_0 e^{-(\beta-\gamma)t}}{S_0 + I_0}\right)^{-(\beta/(\beta-\gamma))},\\
I(t,x) &= I_0 e^{(\delta\eta^2-\gamma)t-\eta x}\left(\frac{I_0 + S_0 e^{-(\beta-\gamma)t}}{S_0 + I_0}\right)^{-(\beta/(\beta-\gamma))},\\
Q(t,x) &= \gamma \int_0^t \left(I_0 e^{(\delta\eta^2-\gamma)\tau-\eta x}\left(\frac{I_0 + S_0 e^{-(\beta-\gamma)\tau}}{S_0 + I_0}\right)^{-(\beta/(\beta-\gamma))}\right) d\tau + Q_0 e^{-\eta x}.
\end{aligned}
\tag{52}
$$

Here, the boundary functions $\Omega_i, i = 1, \ldots, 6$ are provided in (51).

4.2. Transmission Dynamics of COVID-19. Now, we explore the exact solution for the densities of susceptible individuals $S(t, x)$, infected individuals $I(t, x)$, and quarantined individuals $Q(t, x)$, as described in equation (52), to understand the transmission dynamics of COVID-19. We will utilize parameter values taken from relevant literature (see e.g., [17, 18, 39] and references therein): $\delta = 0.2$, $\eta = 0.09$, $\beta = 0.4$, $\gamma = 0.3$, $S_0 = 10^5 - 200 - 50$, $I_0 = 200$, and $Q_0 = 50$. For visualization, we consider a spatial range of $0 \le x \le 10$ and a time interval of $0 \le t \le 100$. We followed Thabet and Kendre [18] and have provided the surface plots for $S(t, x)$, $I(t, x)$, and $Q(t, x)$. The two-dimensional (2-D) plots for $S(t, \overline{x})$, $I(t, \overline{x})$, and $Q(t, \overline{x})$ for some fixed value of $x = \overline{x}$ are also included.

The exact solution (52) for the variables $S(t, x)$, $I(t, x)$, and $Q(t, x)$ is visually presented in Figures 1–6. The surface plots illustrate the densities of $S(t, x)$, $I(t, x)$, and $Q(t, x)$ over a time interval $0 \le t \le 100$ and spatial range $0 \le x \le 10$. Additionally, 2-D plots illustrate the densities of susceptible, infected, and quarantined individuals at fixed spatial

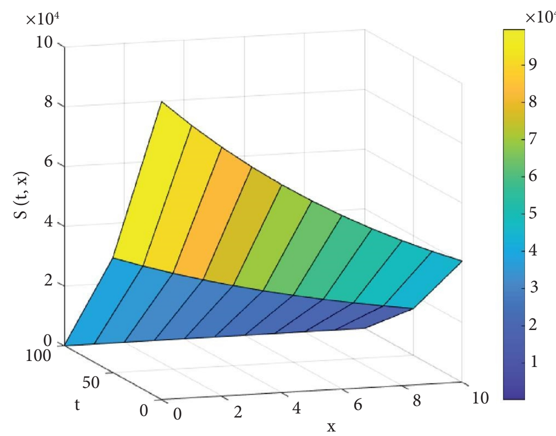

FIGURE 1: The surface plot of $S(t,x)$ with parameters $\delta = 0.2$, $\eta = 0.09$, $\beta = 0.4$, $\gamma = 0.3$, $S_0 = 10^5 - 200 - 50$, $I_0 = 200$, and $Q_0 = 50$ over a time interval $0 \le t \le 100$ and spatial range $0 \le x \le 10$.

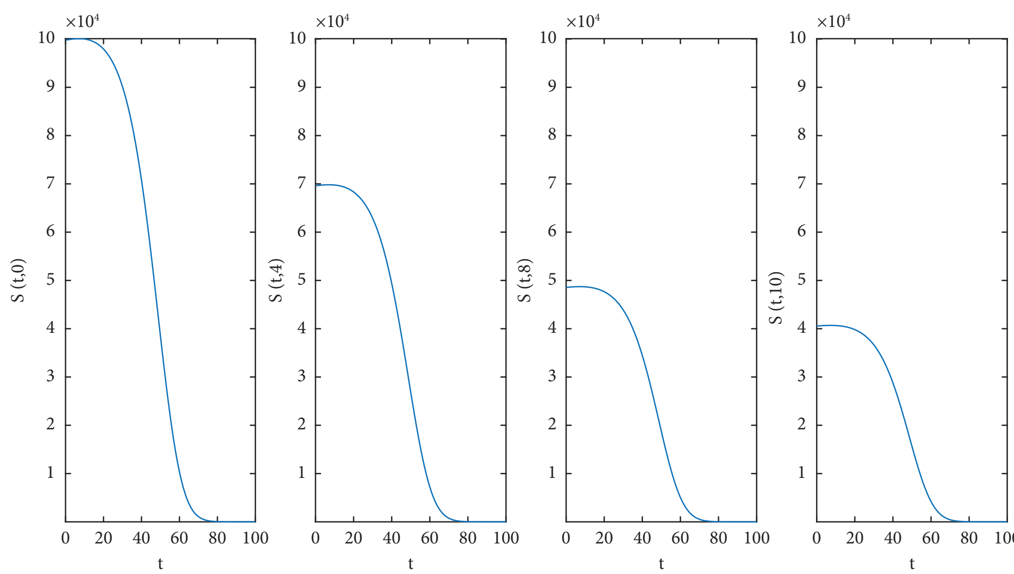

FIGURE 2: The 2-D plots illustrating the densities of susceptible individuals at fixed spatial locations x over a time interval $0 \le t \le 100$. The plots correspond to $x = 0, x = 4, x = 8, x = 10$, with specified parameters and initial conditions: $\delta = 0.2$, $\eta = 0.09$, $\beta = 0.4$, $\gamma = 0.3$, $S_0 = 10^5 - 200 - 50$, $I_0 = 200$, and $Q_0 = 50$.

locations x over the time interval $0 \le t \le 100$. The 2-D plots illustrating the densities of susceptible, infected, and quarantined individuals at the spatial boundaries $x = 0$ and $x = 10$ over the time interval $0 \le t \le 100$ are provided as well. The other fixed spatial positions considered here are $x = 4$ and $x = 8$. It is worth mentioning here that at the boundary $x = 0$, the diffusive SIQ model behaves similarly to the classical SIR model proposed by Kermack and McKendrick [1].

The surface plot illustrating the density of $S(t,x)$, over a time interval $0 \le t \le 100$ and spatial range $0 \le x \le 10$, is provided in Figure 1. The 2-D plots illustrating the densities of susceptible individuals at fixed spatial locations x over a time interval $0 \le t \le 100$ are given in Figure 2. The plots in Figures 1 and 2 illustrate the temporal and spatial dynamics of the density of susceptible individuals. Over time, a decreasing trend in susceptibility is observed, indicating a decline in the density of susceptible individuals. However, this trend varies across space, while susceptibility diminishes rapidly in areas closer to the initial outbreak at $x = 0$, and the decrease is less pronounced in locations farther from the source. The highest susceptibility is consistently observed near the initial outbreak, reflecting the intense transmission dynamics in this region. As spatial distance from the outbreak increases, the rate at which susceptibility decreases slows down.

Next, we shift our focus to the density of infected individuals $I(t,x)$ presented graphically in Figures 3 and 4. Figures 3 and 4 demonstrate an initial increase in the density of infected individuals. This is followed by the attainment of a peak, after which the cases gradually decrease, contributing to the flattening of the curve over time. This observed pattern

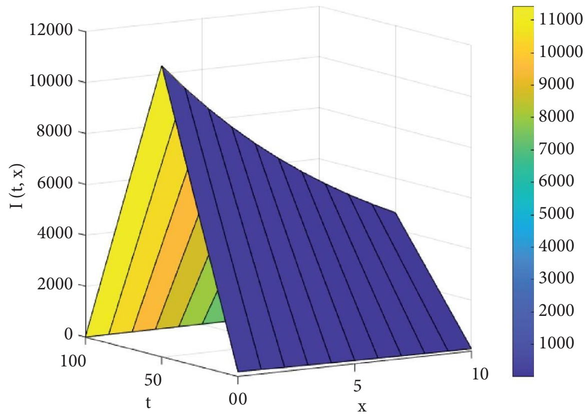

Figure 3: The surface plot of $I(t, x)$ with parameters $\delta = 0.2$, $\eta = 0.09$, $\beta = 0.4$, $\gamma = 0.3$, $S_0 = 10^5 - 200 - 50$, $I_0 = 200$, and $Q_0 = 50$ over a time interval $0 \le t \le 100$ and spatial range $0 \le x \le 10$.

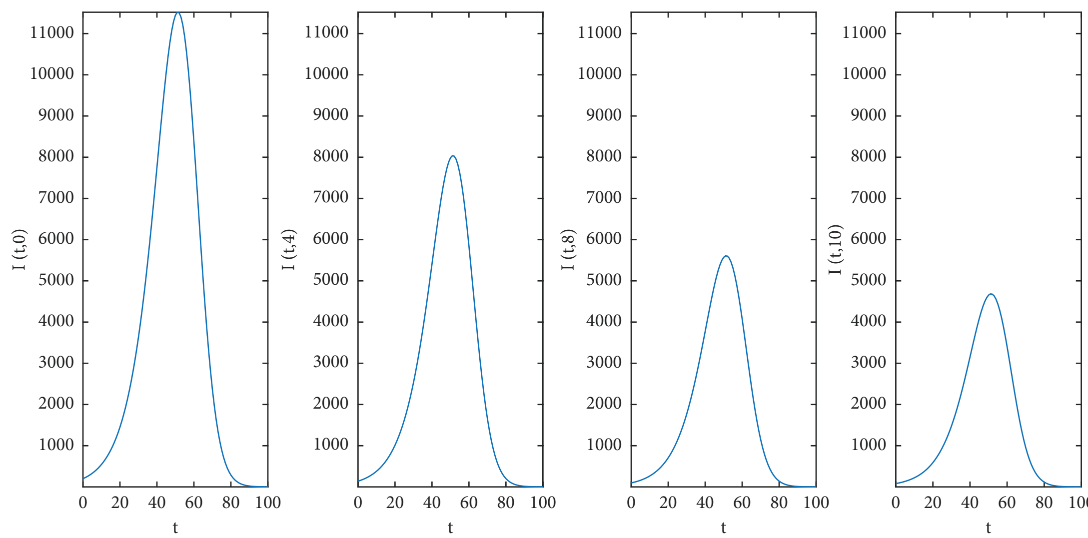

Figure 4: The 2-D plots illustrating the densities of infected individuals at fixed spatial locations x over a time interval $0 \le t \le 100$. The plots correspond to $x = 0, x = 4, x = 8, x = 10$, with specified parameters and initial conditions: $\delta = 0.2$, $\eta = 0.09$, $\beta = 0.4$, $\gamma = 0.3$, $S_0 = 10^5 - 200 - 50$, $I_0 = 200$, and $Q_0 = 50$.

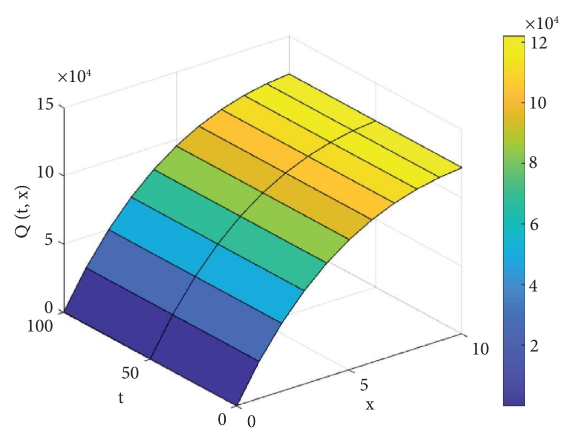

Figure 5: The surface plot of $Q(t, x)$ with parameters $\delta = 0.2$, $\eta = 0.09$, $\beta = 0.4$, $\gamma = 0.3$, $S_0 = 10^5 - 200 - 50$, $I_0 = 200$, and $Q_0 = 50$ over a time interval $0 \le t \le 100$ and spatial range $0 \le x \le 10$.

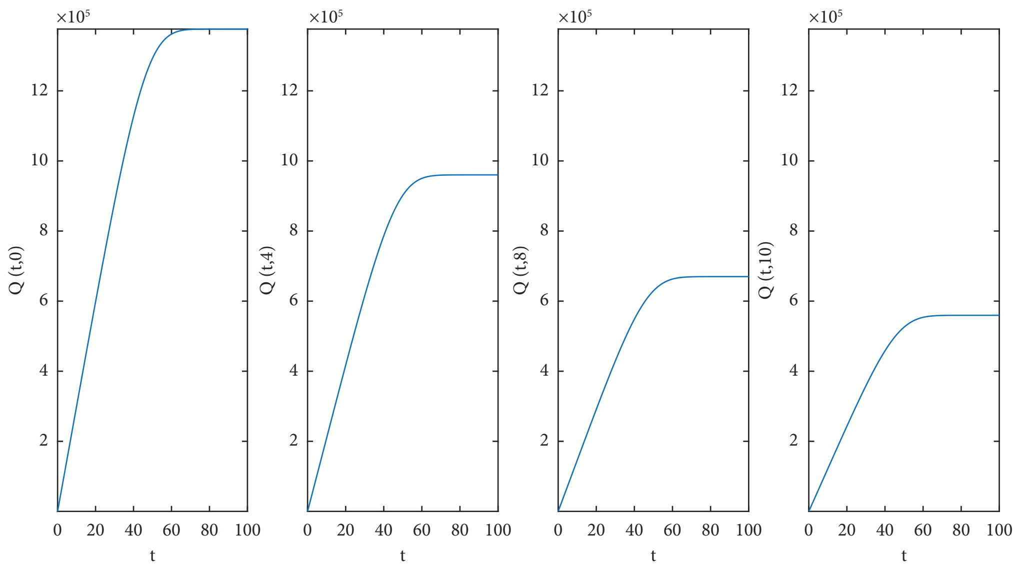

FIGURE 6: The 2-D plots illustrating the densities of quarantined individuals at fixed spatial locations x over a time interval $0 \leq t \leq 100$. The plots correspond to $x = 0, x = 4, x = 8, x = 10$, with specified parameters and initial conditions: $\delta = 0.2$, $\eta = 0.09$, $\beta = 0.4$, $\gamma = 0.3$, $S_0 = 10^5 - 200 - 50$, $I_0 = 200$, and $Q_0 = 50$.

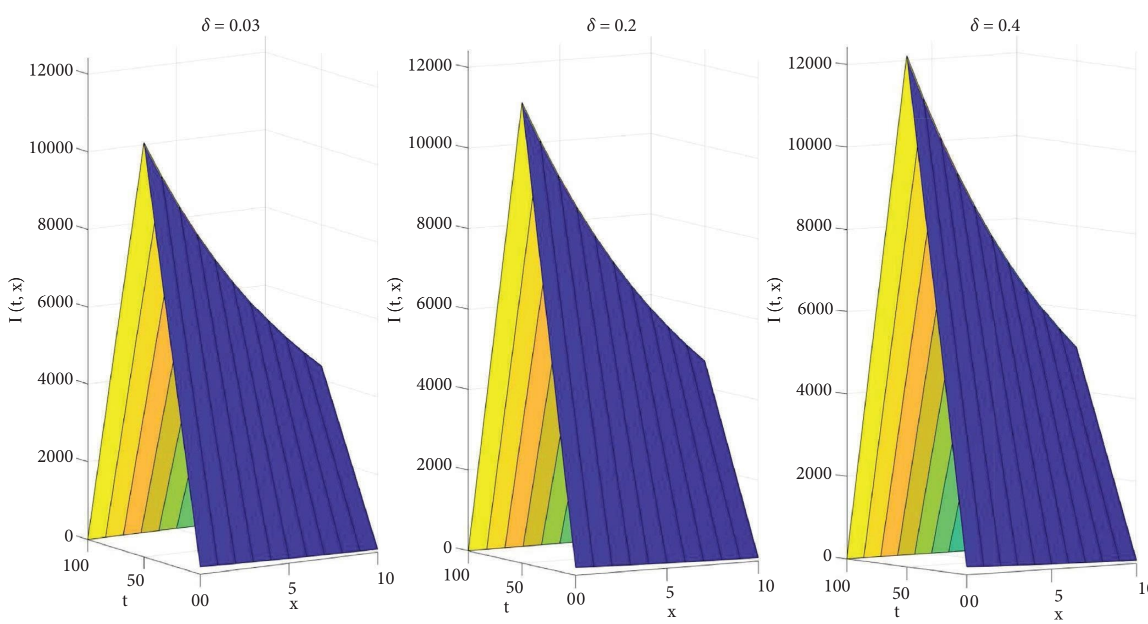

FIGURE 7: The surface plot of $I(t, x)$ to visualize the effect of the diffusion rate on epidemic peak.

is not limited to the source of the disease at $x = 0$ but extends to various locations, reaching even areas more distant from the initial outbreak. Figures 3 and 4 show a decreasing trend in the density of infected individuals $I(t, x)$ as spatial distance increases, and this pattern is consistently observed at each time point. The epidemic peak is highest at the source $x = 0$ of the initial outbreak and is lowest in the farthermost region $x = 10$.Finally, turning our attention to the density of quarantine individuals, the surface plot illustrating the density of $Q(t, x)$, over a time interval $0 \leq t \leq 100$ and spatial range $0 \leq x \leq 10$, is provided in Figure 5. The 2-D plots illustrating the densities of quarantined individuals at fixed spatial locations x over a time interval $0 \leq t \leq 100$ are given in Figure 6. When examining Figures 5 and 6, it is evident that the density of quarantined individuals demonstrates an increasing trend over time. This trend is evident not only at the source of the disease at $x = 0$ but also in other locations and even in areas farther from the initial outbreak. $Q(t, 0)$ is consistently the highest which implies that quarantine measures are implemented more rapidly in areas closer to the initial outbreak, contributing to a higher density of quarantined individuals. The graph of density of quarantined individuals Q follows a lower trajectory for higher values of x. The graphs 5-6 consistently demonstrate

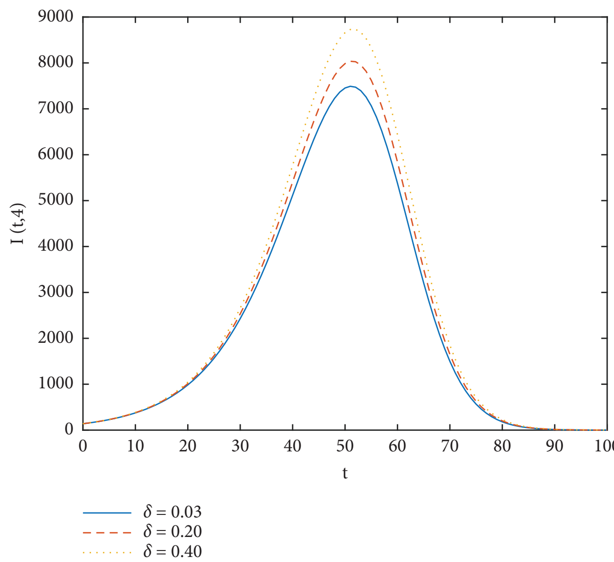

Figure 8: The 2-D plot of $I(t, 4)$ to visualize the effect of the diffusion rate on epidemic peak.

a decreasing trend in the density of quarantined individuals $Q(t, x)$ as spatial distance from the initial outbreak $x = 0$ increases. The highest level of density of quarantined individuals is observed closest to the source, whereas the lowest level is found at locations farther away.

This analysis helps us understand how COVID-19 spreads in different places and over time in the diffusive SIQ model. It shows us the variations in densities of susceptibility, infection, and quarantine individuals, giving us useful insights into how the situation changes across diverse locations and time frames. One can compute the total number of susceptible, infected, and quarantined individual over the space interval $[x_1, x_2]$ where $x_1 < x_2$ following the method outlined by Cherniha and Davydovych [35]. This can be achieved by utilizing the following formulas:

$$\begin{aligned} S(t) &= \int_{x_1}^{x_2} S(t, x)\mathrm{d}x, \\ I(t) &= \int_{x_1}^{x_2} I(t, x)\mathrm{d}x, \\ Q(t) &= \int_{x_1}^{x_2} Q(t, x)\mathrm{d}x. \end{aligned} \tag{53}$$

4.3. Effect of Diffusion Rate on Epidemic Peak. In our analysis of COVID-19 dynamics, we investigate the impact of different diffusion rates on the epidemic peak. This is illustrated by plotting the surface representation of the density of infected individuals, denoted as $I(t, x)$, in Figure 7, for three distinct diffusion rates: $\delta = 0.03, 0.2, 0.4$. The figures clearly depict that as the diffusion rate δ increases, the magnitude of the epidemic peak also rises. This trend holds consistently across various time points t and spatial locations x. To make the visualization easier, we plot the 2-D graphs of $I(t, 4)$ for the three diffusion rates $\delta = 0.03, 0.2, 0.4$ in Figure 8. As δ increases, the graph $I(t, 4)$ shifts upwards.

In the context of COVID-19 spread, varying values of δ influence the epidemic peak. A higher $\delta = 0.4$ is associated with a larger epidemic peak compared to $\delta = 0.2$, while the lowest peak occurs at $\delta = 0.02$. This highlights the sensitivity of the model to spatial spread, with higher diffusion rates leading to increased infection levels and a more pronounced impact at specific time points. Understanding these dynamics is crucial for developing effective strategies to mitigate and manage the spread of COVID-19, emphasizing the pivotal role of spatial factors in controlling transmission dynamics. Spatial movements can be controlled by implementing a border closure policy, a measure actually adopted by many countries to curb COVID-19.

5. Concluding Remarks

Our exploration involved the investigation of the diffusive SIR epidemic model, incorporating diffusion and nonlinear incidence. We provided the reductions and established the exact solutions by utilizing the Lie symmetry method. The understudy model exhibited a four-dimensional Lie algebra. The group-invariant solutions and reductions for the model were established by means of the optimal system of one-dimensional subalgebras of the algebra deduced from the admissible Lie point symmetries. We also made use of the subalgebras which are obtainable by adjoint maps from the optimal system in order to deduce new group-invariant solutions.

We applied the results to the diffusive SIQ model to understand the transmission dynamics of COVID-19. The temporal and spatial dynamics of the density of susceptible individuals indicated a decreasing trend in susceptibility over time. It diminished faster near the source of outbreak and slows down in locations farther from the source. The highest susceptibility was consistently observed near the initial outbreak, and with an increase in spatial distance from the outbreak, the rate at which susceptibility decreased slowed down. The temporal and spatial dynamics of the density of infected individuals demonstrate an initial increase in the density of infected individuals. This was followed by the attainment of a peak, after which the cases gradually decreased to the flattening of the curve over time. A similar pattern was observed at the source of the outbreak and other locations even more distant from the initial outbreak. The epidemic peak was highest at the source of the initial outbreak and was lowest in the farthermost region. The density of quarantined individuals demonstrated an increasing trend over time. This trend was evident at the source of the initial outbreak and in other locations, including the areas farther from the initial outbreak. The graph of density of quarantined individuals was highest at the source of the initial outbreak and followed a lower trajectory in distant locations, indicating quicker implementation of quarantine measures near the source. The highest density of quarantined individuals was observed closest to the source, while the lowest density was found farther away. We also investigated the impact of different diffusion rates on the epidemic peak. The higher value of diffusion rate resulted in a higher epidemic peak. Our study suggests that the implementation of measures such as border closure policies, as seen in various countries, demonstrates the practical application of spatial factors in controlling transmission dynamics.

Data Availability

Data sharing is not applicable to this article as no datasets were generated or analyzed during the current study.

Disclosure

The University of the Witwatersrand is part of Wiley's agreement with South African National Library and Information Consortium (SANLiC) which covers open access article publication charges.

Conflicts of Interest

The authors declare that they have no conflicts of interest.

Acknowledgments

Fazal M. Mahomed, affiliated with the University of the Witwatersrand, serves as the corresponding author and is entitled to the associated funding. The open access charges are paid as per the agreement between University of the Witwatersrand, Johannesburg and Wiley.

References

[1] W. O. Kermack and A. G. McKendrick, "Contributions to the mathematical theory of epidemics II. The problem of endemicity," *Proceedings of the Royal Society of London*, vol. 138, no. 834, pp. 55–83, 1932.

[2] J. V. Noble, "Geographic and temporal development of plagues," *Nature*, vol. 250, no. 5469, pp. 726–729, 1974.

[3] A. Källén, "Thresholds and travelling waves in an epidemic model for rabies," *Nonlinear Analysis: Theory, Methods and Applications*, vol. 8, no. 8, pp. 851–856, 1984.

[4] A. Källén, P. Arcuri, and J. D. Murray, "A simple model for the spatial spread and control of rabies," *Journal of Theoretical Biology*, vol. 116, no. 3, pp. 377–393, 1985.

[5] J. D. Murray, E. A. Stanley, and D. L. Brown, "On the spatial spread of rabies among foxes," *Proceedings of the Royal Society of London-Series B: Biological Sciences*, vol. 229, no. 1255, pp. 111–150, 1986.

[6] J. D. Murray and W. L. Seward, "On the spatial spread of rabies among foxes with immunity," *Journal of Theoretical Biology*, vol. 156, no. 3, pp. 327–348, 1992.

[7] R. S. Cantrell and C. Cosner, *Spatial Ecology via Reaction-Diffusion Equations*, John Wiley and Sons, Hoboken, NJ, USA, 2004.

[8] V. Davydovych, V. Dutka, and R. Cherniha, "Reaction-diffusion equations in mathematical models arising in epidemiology," *Symmetry*, vol. 15, no. 11, p. 2025, 2023.

[9] S. C. Fu, "Traveling waves for a diffusive SIR model with delay," *Journal of Mathematical Analysis and Applications*, vol. 435, no. 1, pp. 20–37, 2016.

[10] J. Yang, S. Liang, and Y. Zhang, "Travelling waves of a delayed SIR epidemic model with nonlinear incidence rate and spatial diffusion," *PLoS One*, vol. 6, no. 6, p. e21128, Article ID e21128, 2011.

[11] K. Zhou, M. Han, and Q. Wang, "Traveling wave solutions for a delayed diffusive SIR epidemic model with nonlinear incidence rate and external supplies," *Mathematical Methods in the Applied Sciences*, vol. 40, no. 7, pp. 2772–2783, 2017.

[12] Z. Zhen, J. Wei, L. Tian, J. Zhou, and W. Chen, "Wave propagation in a diffusive SIR epidemic model with spatiotemporal delay," *Mathematical Methods in the Applied Sciences*, vol. 41, no. 16, pp. 7074–7098, 2018.

[13] E. Avila-Vales, G. E. Garcia-Almeida, and A. G. Perez, "Qualitative analysis of a diffusive SIR epidemic model with saturated incidence rate in a heterogeneous environment," *Journal of Mathematical Analysis and Applications*, vol. 503, no. 1, Article ID 125295, 2021.

[14] Z. C. Wang, L. Zhang, and X. Q. Zhao, "Time periodic traveling waves for a periodic and diffusive SIR epidemic model," *Journal of Dynamics and Differential Equations*, vol. 30, no. 1, pp. 379–403, 2018.

[15] J. Zhou, L. Song, J. Wei, and H. Xu, "Critical traveling waves in a diffusive disease model," *Journal of Mathematical Analysis and Applications*, vol. 476, no. 2, pp. 522–538, 2019.

[16] L. Zhao, Z. C. Wang, and S. Ruan, "Traveling wave solutions in a two-group SIR epidemic model with constant recruitment," *Journal of Mathematical Biology*, vol. 77, no. 6-7, pp. 1871–1915, 2018.

[17] Q. Cao, Y. Liu, and W. Yang, "Global dynamics of a diffusive SIR epidemic model with saturated incidence rate and discontinuous treatments," *International journal of dynamics and control*, vol. 10, no. 6, pp. 1770–1777, 2022.

[18] H. Thabet and S. Kendre, "Conformable mathematical modeling of the COVID-19 transmission dynamics: a more general study," *Mathematical Methods in the Applied Sciences*, vol. 46, no. 17, pp. 18126–18149, 2023.

[19] L. V. Ovsiannikov, *Group Analysis of Differential Equations*, Academic Press, New York, USA, 1982.

[20] G. W. Bluman and S. Kumei, *Symmetries and Differential Equations*, Springer, New York, USA, 1989.

[21] P. J. Olver, *Applications of Lie Groups to Differential Equations*, Springer, Verlag, New York, NY, USA, 2nd edition, 1993.

[22] N. H. Ibragimov, Ed., *CRC Handbook of Lie Group Analysis of Differential Equations*, CRC Press, Boca Raton, FL, USA, 1996.

[23] D. J. Arrigo, *Symmetry Analysis of Differential Equations: An Introduction*, John Wiley and Sons, Hoboken, NJ, USA, 2015.

[24] R. Cherniha, M. Serov, and O. Pliukhin, *Nonlinear Reaction-Diffusion-Convection Equations: Lie and Conditional Symmetry, Exact Solutions and Their Applications*, CRC Press, Boca Raton, FL, USA, 2017.

[25] W. Hereman, "Symbolic software for lie symmetry analysis. In: CRC handbook of lie group analysis of differential equations," in *Ed.: N. H. Ibragimov, New Trends in Theoretical Developments and Computational Methods*, vol. 3, pp. 367–413, CRC Press, Boca Raton, FL, USA, 1996.

[26] W. Hereman, "Review of symbolic software for Lie symmetry analysis," *Mathematical and Computer Modelling*, vol. 25, no. 8-9, pp. 115–132, 1997.

[27] T. M. Rocha Filho and A. Figueiredo, "[SADE] A Maple package for the symmetry analysis of differential equations," *Computer Physics Communications*, vol. 182, no. 2, pp. 467–476, 2011.

[28] A. F. Cheviakov, "GeM software package for computation of symmetries and conservation laws of differential equations," *Computer Physics Communications*, vol. 176, no. 1, pp. 48–61, 2007.

[29] B. Champagne, W. Hereman, and P. Winternitz, "The computer calculation of Lie point symmetries of large systems of differential equations," *Computer Physics Communications*, vol. 66, no. 2-3, pp. 319–340, 1991.

[30] W. Hereman, "SYMMGRP MAX and other symbolic programs for lie symmetry analysis of partial differential equation," *Lectures in Applied Mathematics*, vol. 29, pp. 241–257, 1993.

[31] I. G. Lisle and S. L. T. Huang, "Algorithmic calculus for Lie determining systems," *Journal of Symbolic Computation*, vol. 79, pp. 482–498, 2017.

[32] I. L. Freire and M. Torrisi, "Similarity solutions for systems arising from an Aedes aegypti model," *Communications in Nonlinear Science and Numerical Simulation*, vol. 19, no. 4, pp. 872–879, 2014.

[33] F. Bacani, S. Dimas, I. L. Freire, N. A. Maidana, and M. Torrisi, "Mathematical modelling for the transmission of dengue: symmetry and travelling wave analysis," *Nonlinear Analysis: Real World Applications*, vol. 41, pp. 269–287, 2018.

[34] Ö. Orhan, M. Torrisi, and R. Tracinà, "Group methods applied to a reaction-diffusion system generalizing Proteus Mirabilis models," *Communications in Nonlinear Science and Numerical Simulation*, vol. 70, pp. 223–233, 2019.

[35] R. M. Cherniha and V. V. Davydovych, "A reaction-diffusion system with cross-diffusion: lie symmetry, exact solutions and their applications in the pandemic modelling," *European Journal of Applied Mathematics*, vol. 33, no. 5, pp. 785–802, 2022.

[36] W. I. Fushchych and R. M. Cherniha, "Galilei-invariant nonlinear systems of evolution equations," *Journal of Physics A: Mathematical and General*, vol. 28, no. 19, pp. 5569–5579, 1995.

[37] J. Patera and P. Winternitz, "Subalgebras of real three-and four-dimensional Lie algebras," *Journal of Mathematical Physics*, vol. 18, no. 7, pp. 1449–1455, 1977.

[38] H. Hethcote, M. Zhien, and L. Shengbing, "Effects of quarantine in six endemic models for infectious diseases," *Mathematical Biosciences*, vol. 180, no. 1-2, pp. 141–160, 2002.

[39] R. Naz and M. Al-Raeei, "Analysis of transmission dynamics of COVID-19 via closed-form solutions of a susceptible-infectious-quarantined-diseased model with a quarantine-adjusted incidence function," *Mathematical Methods in the Applied Sciences*, vol. 44, no. 14, pp. 11196–11210, 2021.